ACSNANO
www.acsnano.org
ARTICLE

Tunable Affinity and Molecular Architecture Lead to Diverse Self-Assembled Supramolecular Structures in Thin Films

Chih-Hao Hsu,[†,⊥] Xue-Hui Dong,[†,⊥] Zhiwei Lin,[†] Bo Ni,[†] Pengtao Lu,[†] Zhang Jiang,[‡] Ding Tian,[†] An-Chang Shi,[*,§] Edwin L. Thomas,[*,∥] and Stephen Z. D. Cheng[*,†]

[†]Department of Polymer Science, College of Polymer Science and Polymer Engineering, The University of Akron, Akron, Ohio 44325, United States

[‡]X-ray Science Division, Advanced Photon Source, Argonne National Laboratory, 9700 South Cass Avenue, Argonne, Illinois 60439, United States

[§]Department of Physics and Astronomy, McMaster University, Hamilton, Ontario, Canada, L8S 4M1

[∥]Department of Materials Science and Nano Engineering and Department of Chemical and Biomolecular Engineering, Brown School of Engineering, Rice University, Houston, Texas 77251, United States

Supporting Information

ABSTRACT: The self-assembly behavior of specifically designed giant surfactants is systematically studied in thin films using grazing incidence X-ray scattering and transmission electron microscopy, focusing on the effects of molecular nanoparticle (MNP) functionalities and molecular architectures on nanostructure formation. Two MNPs with different surface functionalities, *i.e.*, hydrophilic carboxylic acid functionalized [60]fullerene (AC_{60}) and omniphobic fluorinated polyhedral oligomeric silsesquioxane (FPOSS), are utilized as the head portions of the giant surfactants. By covalently tethering these functional MNPs onto the end point or junction point of polystyrene-*block*-poly(ethylene oxide) (PS-*b*-PEO) diblock copolymer, linear and star-like giant surfactants with different molecular architectures are constructed. With fixed length of the PEO block, changing the molecular weight of the PS block leads to the formation of various ordered phases and phase transitions. Due to the distinct affinity, the AC_{60}-based and FPOSS-based giant surfactants form two- or three-component morphologies, respectively. A stretching parameter for the PS block is introduced to characterize the PS chain conformation in the different morphologies. The highly diverse self-assembled nanostructures with high etch resistance between components in small dimensions obtained from the giant surfactant thin films suggest that these macromolecules could provide a promising and robust platform for nanolithography applications.

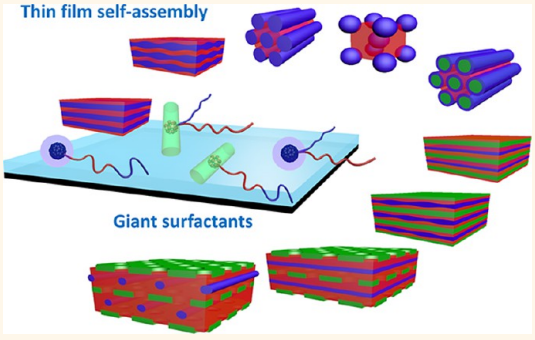

KEYWORDS: *surface functionality, nanoparticles, molecular architecture, self-assembly, thin film*

Engineering ordered patterns with small feature sizes over large areas presents a critical challenge for the development of future devices. Top-down lithographic techniques have been the method of choice.[1] The dramatic increase of the cost-effectiveness ratio for pushing current practical limits in the top-down lithographic technology motivates intensive efforts in finding alternative approaches.[2,3] Among the many bottom-up methods, the self-assembly of block copolymers provides a promising technique for next-generation device fabrication.[4,5] Using self-organization or directed assembly, ordered patterns with desirable properties, *e.g.*, morphology, domain orientation, and domain spacing, can be obtained by adjusting the molecular design.[6−8] Several challenges, nevertheless, still remain: (1) generating morphologies with long-range order and small feature sizes (*e.g.*, <22 nm); (2) obtaining sharp interfaces with high lithographic contrast; and (3) enhancing etch selectivity and resistance between different components of the nanostructures. For ordered morphologies of diblock copolymers, the domain size is determined by the monomer−monomer interaction and overall molecular weight, $d \approx \chi^{1/6}N^{2/3}$, where N is overall degree of polymerization and χ is the Flory−Huggins interaction parameter.[7,9] On the other hand, the product χN determines the ordered transition of diblock copolymers. Since the dimension of self-assembled patterns is proportional to $N^{2/3}$

Received: September 25, 2015
Accepted: December 1, 2015
Published: December 1, 2015

DOI: 10.1021/acsnano.5b06038
ACS Nano 2016, 10, 919−929

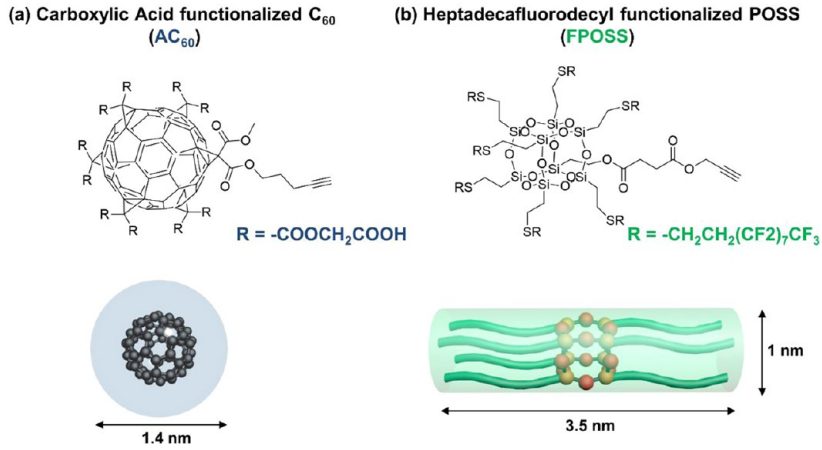

Figure 1. Chemical structures and schematic illustrations of (a) AC_{60} and (b) FPOSS MNPs. The alkyne groups are the covalent tether points for the MNPs. The amorphous carboxylic acid functional groups of AC_{60} are depicted by a blue shell, while the mesomorphic fluorinated chains of FPOSS are depicted by a green cylinder. FPOSS MNP dimensions are determined from wide-angle X-ray diffraction experiments (Figure S1).

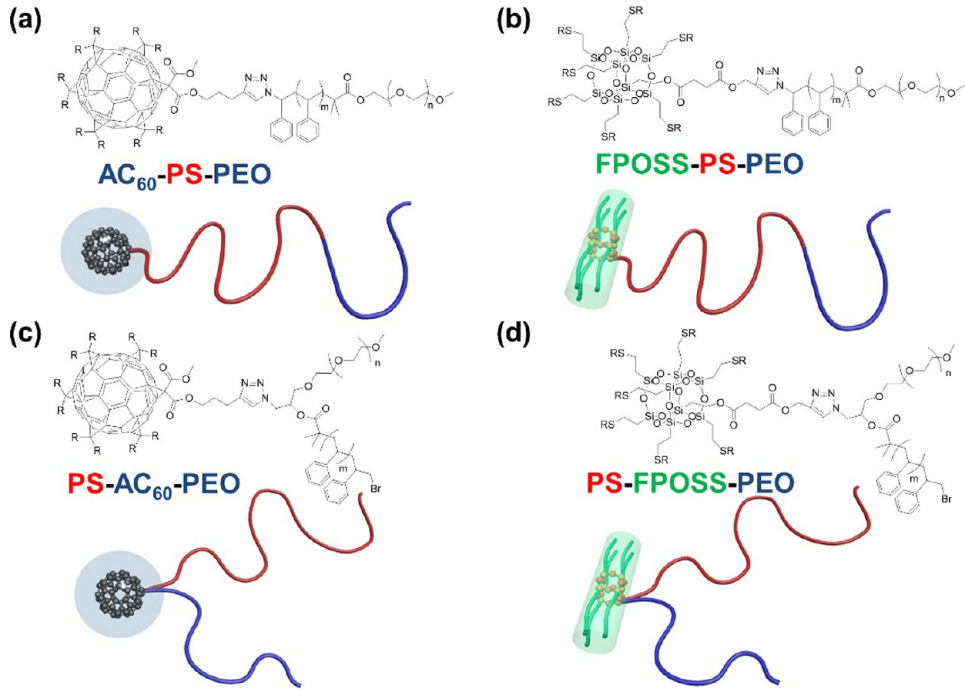

Figure 2. Chemical structure and molecular architecture of the giant surfactants: (a) linear AC_{60}-PS-PEO with hydrophilic−hydrophobic−hydrophilic property, (b) linear FPOSS-PS-PEO with omniphobic−hydrophobic−hydrophilic property, (c) star-like PS-AC_{60}-PEO, and (d) star-like PS-FPOSS-PEO. Hydrophilic components are represented in blue, hydrophobic components in red, and omniphobic components in green.

in the strong segregation region,[10,11] a low N to achieve smaller domain sizes consequently requires a very high effective χ. The interactions between most conventional polymer blocks, unfortunately, are usually weak. Therefore, obtaining ordered morphologies from block copolymers usually requires sufficiently high molecular weight. The design of novel monomers with large χ values represents a straightforward solution.[12−14] Replacing one of the linear blocks with nonlinear topologies, e.g., hyperbranched, cyclic, or dendritic, has also been shown to result in phase separation at reduced feature sizes.[15−18] These approaches, however, usually require complex syntheses and are difficult to be widely adopted.

Computer simulation has manifested that tethering nanoparticles as additional building blocks to polymers could result in various ordered hierarchical structures.[19,20] In the past few years, we have demonstrated that the self-assembly of giant surfactants could provide a platform for engineering nanopatterns with sub-10 nm feature sizes.[21,22] This class of macromolecules consists of compact and rigid molecular nanoparticles (MNPs), *e.g.*, precisely surface-functionalized [60]fullerene (C_{60}) or polyhedral oligomeric silsesquioxane (POSS), as the head portion(s) and flexible polymer chains as the tail portion(s).[21,23] To a large extent, they resemble the general geometrical features of small molecular surfactants, yet with somewhat amplified sizes and controllable local geo-

DOI: 10.1021/acsnano.5b06038
ACS Nano 2016, 10, 919−929

Table 1. Summary of Molecular Compositions and Self-Assembled Morphologies of the Giant Surfactants

	sample[a]	topology	$M_{w,PS}$[b]	$M_{w,PEO}$[b]	PDI[c]	f_{MNP}[d]	f_{PS}[d]	f_{PEO}[d]	$\chi N_{PS/PEO}$[e]	bulk morphology[f]	thin film morphology[g]
A1	AC_{60}-PS_{28}-PEO_{45}	linear	2800	2000	1.10	0.23	0.46	0.31	3.4	LAM	LAM
A2	AC_{60}-PS_{52}-PEO_{45}	linear	5200	2000	1.09	0.16	0.61	0.23	4.5	DG	ML
A3	AC_{60}-PS_{64}-PEO_{45}	linear	6400	2000	1.06	0.14	0.66	0.20	5.1	HEX	HEX
A4	AC_{60}-PS_{78}-PEO_{45}	linear	7800	2000	1.11	0.12	0.71	0.17	5.8	HEX	HEX
A5	AC_{60}-PS_{151}-PEO_{45}	linear	15100	2000	1.13	0.08	0.82	0.10	9.2	HEX	BCC
A6	PS_{50}-AC_{60}-PEO_{45}	star-like	5000	2000	1.10	0.17	0.60	0.23	4.5	LAM	LAM
A7	PS_{78}-AC_{60}-PEO_{45}	star-like	7800	2000	1.09	0.12	0.71	0.17	5.8	HEX	HEX
F1	FPOSS-PS_{28}-PEO_{45}	linear	2800	2000	1.10	0.32	0.41	0.27	3.4	LAM_3	UL_3/LAM_3
F2	FPOSS-PS_{52}-PEO_{45}	linear	5200	2000	1.09	0.24	0.56	0.20	4.5	LAM_3	LAM_3
F3	FPOSS -PS_{64}-PEO_{45}	linear	6400	2000	1.06	0.21	0.61	0.18	5.1	LAM_3	PL_3
F4	FPOSS -PS_{78}-PEO_{45}	linear	7800	2000	1.11	0.18	0.66	0.16	5.8	HEX_3	CPL_3
F5	FPOSS -PS_{151}-PEO_{45}	linear	15100	2000	1.13	0.11	0.79	0.10	9.2	HEX_3	CPL_3
F6	PS_{50}- FPOSS -PEO_{45}	star-like	5000	2000	1.10	0.24	0.55	0.21	4.5	LAM_3	CSC
F7	PS_{78}- FPOSS -PEO_{45}	star-like	7800	2000	1.09	0.18	0.66	0.16	5.8	LAM_3	CSC

[a]Sample labels: the subscripts represent the degree of polymerization, *N*. [b]Molecular weight calculated from ^{1}H NMR. [c]Polydispersity index measured by SEC. [d]Volume fraction based on molecular weights and densities (see details in the SI). [e]The product of degree of polymerization and Flory–Huggins interaction parameter at 120 °C (annealing temperature, see details in the SI). [f]Bulk morphology determined by SAXS and TEM at 25 °C. [g]Corresponding thin film morphology at 25 °C, determined by GISAXS and TEM.

metries. A simple and representative example is single-head/single-tail giant surfactants, which can assemble into a variety of ordered structures similar to those found in flexible diblock copolymers in the bulk and thin films.[22] The collective secondary interactions and geometrical constraints greatly enhance the effective immiscibility,[24] leading to the formation of stable ordered structures with domain size around or less than 10 nm.[22] Furthermore, the outstanding electronic properties of C_{60} and the excellent etch-resistance of POSS endow the giant surfactants with both scientific and technologic relevance.

Introducing a block copolymer tail to the giant surfactants can expand the diversity of these macromolecules tremendously, thus promoting the variety and complexity of self-assembled structures.[22,25−27] Different from the simple single-head/single-tail giant surfactants, conjugating MNPs with block copolymers provides two additional variables for molecular design: chain architecture and affinity. By tethering MNPs to specific positions of block copolymers, topological isomers can be generated that possess the same composition but have different architectures.[22,27,28] On the other hand, adjusting the surface functionality of MNPs could tune the relative interactions between the MNP and the polymeric blocks, leading to controllable partitions of the MNP in different domains. Giant surfactants tethered with block copolymers thus provide a unique system to highlight the importance of these variables on self-assembly. Recently, we have designed and synthesized a library of giant surfactants by attaching a carboxylic acid-functionalized C_{60} (AC_{60}) or a heptadecafluorodecyl-functionalized POSS (FPOSS) (Figure 1) onto a polystyrene-*block*-poly(ethylene oxide) (PS-*b*-PEO) diblock copolymer at the end of PS block (AC_{60}-PS-PEO and FPOSS-PS-PEO) or the junction point (PS-FPOSS-PEO and PS-AC_{60}-PEO) with linear and star-like architectures, respectively (Figure 2).[27,29] Rich self-assembled structures have been identified in the bulk.[30,31] The differences in architecture and affinity lead to distinct molecular arrangements.

In this work, we will focus on the self-assembly of these giant surfactants in thin (∼100 nm) films. Due to the geometrical confinement, diverse self-assembled structures, many of which are not available in bulk, were observed. Specifically, the different affinity of the head leads to the formation of two-component and three-component morphologies in the AC_{60}-based and FPOSS-based giant surfactants, respectively. With a fixed molecular weight of the PEO block, the length of the PS block acts as the prominent factor to control the self-assembled morphologies. The importance of the chain conformation of the PS block in the morphology transition and the topological effect was carefully investigated.

RESULTS AND DISCUSSION

The giant surfactants are prepared by a combination of controlled living radical polymerization and "click" chemistry, with well-defined structures and narrow molecular weight distributions. Details on the synthetic routes and polymerizations have been recently reported[30−32] and are briefly described in the Supporting Information (SI). The degree of polymerization of the PEO block is fixed at 45, while the PS block length varies. The volume fraction of PS (f_{PS}) ranges between 0.4 and 0.8 for the linear giant surfactants and from 0.6 to 0.7 for the star-like ones (Table 1). The overall molecular weights of PS-*b*-PEO copolymers were specifically controlled within the weak phase separation region (*i.e.*, $\chi N < 10$) to highlight the importance of MNPs in promoting nanophase separation.

Microdomain Structures in Thin Films of Linear Giant Surfactants. The grazing incidence small-angle X-ray scattering (GISAXS) pattern of **A1** (Figure 3a) shows clear (001) and (002) diffraction peaks along the q_z direction at $q_y = 0$ nm^{-1}, representing a significant order along the film normal direction. The appearance of only (00*l*) diffractions indicates that **A1** ($f_{PS} = 0.46$) forms flat-on parallel lamellae (LAM) with a long period of 7.9 nm. On the other hand, the GISAXS pattern of **A2** (Figure 3b) shows diffractions along the q_z direction at both $q_y = 0$ and 0.55 nm^{-1}, suggesting flat-on modulated lamellae (ML) with structual correlations between the layers and the rectangular lattice parameters of $a = 11.3$ nm and $b = 17.8$ nm. The $d_{(020)}$ of 8.9 nm for the ML structure corresponds to the distance bewteen neighboring hydrophilic (or hydrophobic) layers. Due to the layered geometry, no contrast is observed in the plan-view TEM bright field (BF) images of **A1** and **A2**. Instead, the corresponding cross-sectional images of **A1** and **A2**

DOI: 10.1021/acsnano.5b06038
ACS Nano 2016, 10, 919−929

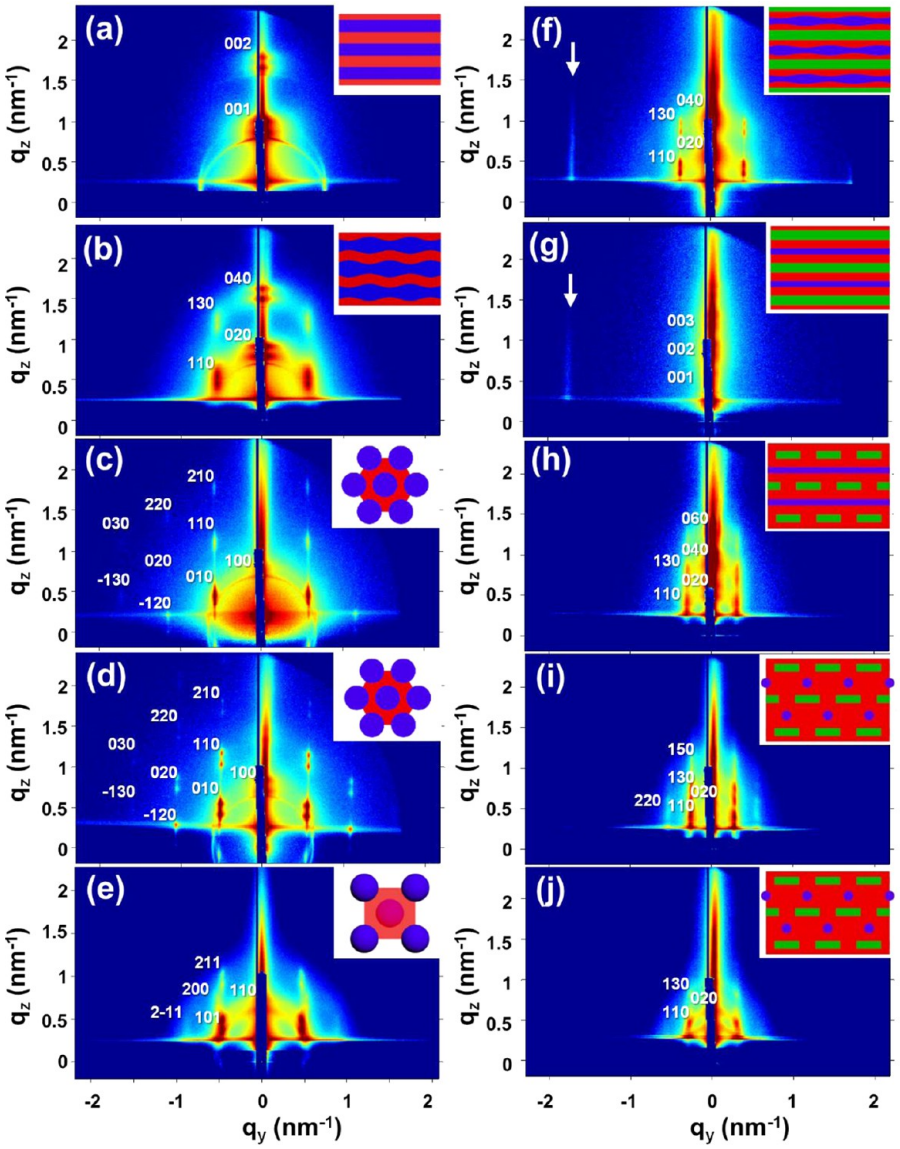

Figure 3. GISAXS patterns at the incident angle of 0.20° of linear AC_{60}-based giant surfactants (a) A1, (b) A2, (c) A3, (d) A4, and (e) A5 and linear FPOSS-based giant surfactants (f) F1, (g) F2, (h) F3, (i) F4, and (j) F5. The insets represent cross-sectional illustrations for each structure with AC_{60} and PEO in blue, PS in red, and FPOSS in green.

(Figure 4a and b) confirm that the PEO/AC_{60} domain (dark regions) transfers from flat layers to modulated layers. Remarkably, the sample **A2** forms a double-gyroid (DG) structure in the bulk state.[30] The formation of ML in the thin film could thus be attributed to the geometrical confinement along the film normal direction, leading to a corresponding frustrated phase of the three-dimensionally (3D) stable bulk DG structure. Hexagonally packed cylinders (HEX) form (Figure 3c and d) with further increasing f_{PS} (**A3** and **A4**). The hexagonal lattice is oriented with its [10] direction parallel to the substrate, while the [21] direction is perpendicular to the substrate.[33] The corresponding dimensions of HEX for **A3** and **A4** are a = 10.8 and 11.7 nm, respectively. Plan-view TEM BF images of **A3** and **A4** (Figure 4c and d) reveal that the PEO/AC_{60} blocks form cylinders embedded in the PS matrix. For the sample with the highest f_{PS} (**A5**), the GISAXS pattern (Figure 3e) shows diffractions along the q_z direction at q_y = 0.46 and 0.53 nm^{-1}, corresponding to d_1 = 13.5 nm and d_2 = 11.7 nm. The ratio of d_1/d_2 is 1.154, which is a characteristic of body-centered cubic (BCC) morphology with the [110] direction perpendicular to the substrate.[34,35] The plan-view TEM BF image of **A5** (Figure 4e) confirms that the PEO/AC_{60} blocks form spherical domains in the PS matrix with a BCC supramolecular lattice.

The TEM BF images suggest that the AC_{60} MNPs and the PEO blocks form a heterogeneous hydrophilic domain in all the AC_{60}-based giant surfactants. In addition, no diffraction patterns corresponding to the ordered packing of AC_{60} MNPs are observed in both GISAXS and grazing incidence wide-angle X-ray scattering (GIWAXS) (Figure S2a–e), indicating that the AC_{60} MNPs are in a disordered state. In addition, the Scherrer–Debye rings with intensity concertrated in the specular direction (Figure 3a–e) have the same q value of the first-order diffraction along the q_z direction at q_y = 0 nm^{-1}, indicating they can be attributed to the correlation between the AC_{60} MNPs in neighboring hydrophilic domains. AC_{60} MNPs are believed to adopt a nonuniform distribution (Scherrer–Debye rings) with the majority locating close to the

DOI: 10.1021/acsnano.5b06038
ACS Nano 2016, 10, 919–929

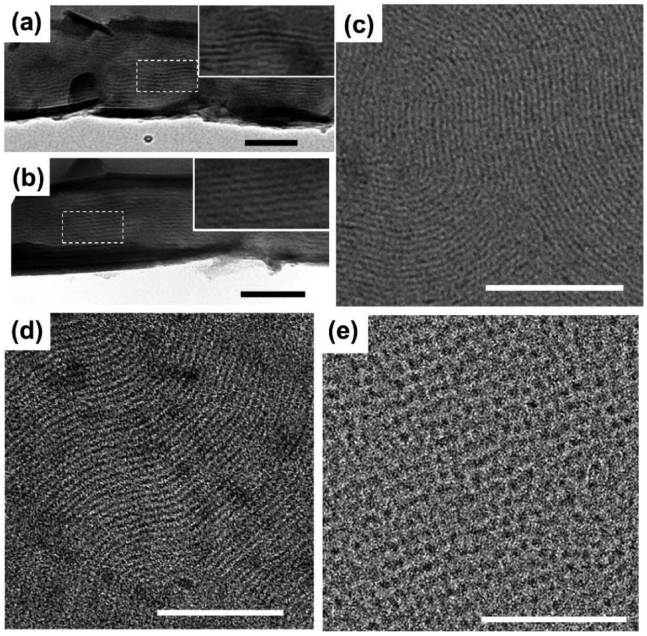

Figure 4. Set of TEM BF images of the linear AC_{60}-based giant surfactants. Cross-sectional images of A1 (a) and A2 (b). The insets are the enlarged images of the marked regions. Plan-view images of A3 (c), A4 (d), and A5 (e). TEM samples were stained by OsO_4, with the AC_{60}/PEO domain in dark gray and the PS domain in light gray. Black and white scale bars: 100 nm.

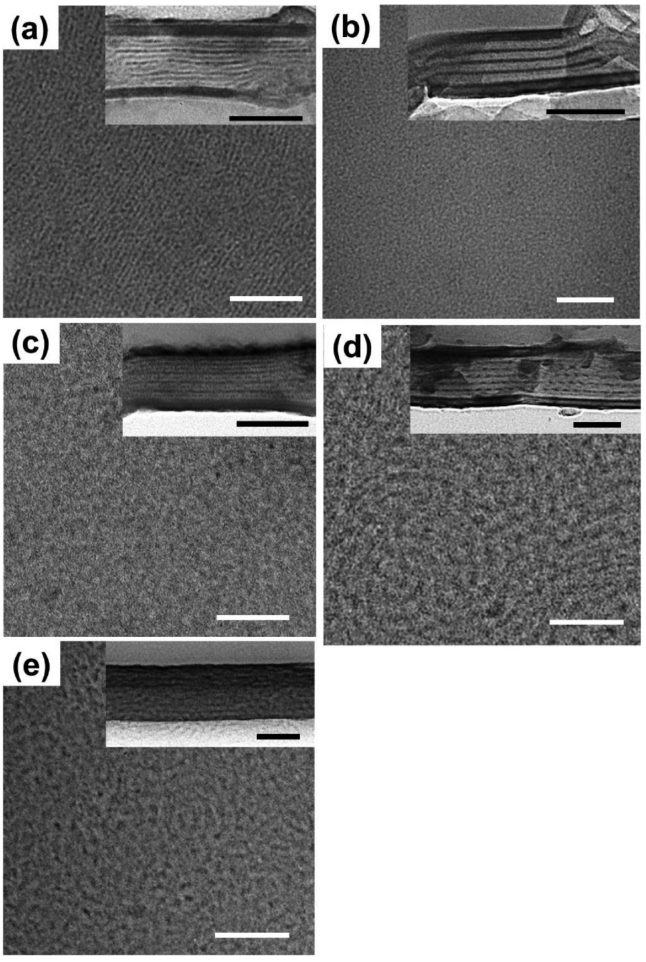

Figure 5. Set of TEM BF images of linear FPOSS-based giant surfactants. Plan-view images of F1 (a), F2 (b), F3 (c), F4 (d), and F5 (e). Insets are the corresponding cross-sectional TEM images. TEM samples were stained by RuO_4, with the PEO domain in dark gray, the FPOSS domain in gray, and the PS domain in light gray. Black and white scale bars: 100 nm.

PEO/PS interface due to the chemical linkage between the AC_{60} and the PS blocks. The hydrophilic−hydrophobic−hydrophilic (A−B−A′) nature of the AC_{60}-PS-PEO samples results in two-component strucutures with a sequence of LAM → ML → HEX → BCC with increasing f_{PS}.

In contrast, the linear FPOSS-based giant surfactants generate a series of more complex morphologies because of their omniphobic−hydrophobic−hydrophilic (A−B−C) nature. Besides the distinct affinity, FPOSS has been found to form a mesomorphic phase (Figure S1), which could enhance the phase separation of the tethered PS and PEO blocks. The GISAXS patterns of these FPOSS-based giant surfactants are shown in Figure 3f to j. The strong diffractions along the q_z direction at $q_y = 0$ nm^{-1} in Figure 3f indicate **F1** forms a three-component lamellar morphology (LAM_3) with a long period of 14.0 nm. Meanwhile, the diffractions along the q_z direction at q_y = 0.39 and 0.78 nm^{-1} represent an additional centered rectangular supramolecular lattice with a = 16.1 nm and b = 24.0 nm. The streak/cylinder-like PEO domain is observed in the plan-view image of **F1** (Figure 5a), while an undulated PEO domain (dark) and the continuous FPOSS domain (gray) appear in the corresponding cross-sectional TEM BF image (inset of Figure 5a). The self-assembled structure of **F1** is thus a mixture of LAM_3 and three-component undulated lamellae (UL_3). UL_3 consists of undulated PEO layers in the PS matrix sandwiched between the FPOSS layers. The composition of **F1** is believed to be close to the phase boundary of the LAM_3 and UL_3 structures. Only diffractions along the q_z direction at $q_y = 0$ nm^{-1} are observed in the GISAXS pattern of **F2** (Figure 3g), indicating a simple LAM_3 morphology (c = 17.0 nm), with each component forming an individual layer. The plan-view TEM BF image (Figure 5b) is featureless due to the flat-on lamellar geometry, while the corresponding cross-sectional image (inset of Figure 5b) clearly shows the LAM_3 morphology with an ABCBA packing scheme.

On further increasing the f_{PS}, the samples **F3**, **F4**, and **F5** exhibit distinct GISAXS patterns (Figure 3h−j) from those of **F1** and **F2**, implying the occurrence of more ordered phases. These structures share similar in-plane and out-of-plane periodicities, among which **F4** possesses the highest order. The plan-view TEM BF image of **F3** shows a perforated FPOSS (net-like gray domain)[36,37] (Figure 5c), and the corresponding cross-sectional image shows a perforated FPOSS (broken gray domain)[38] penetrated by the PS domain and further sandwiched by the layered PEO (continuous dark domain) (inset of Figure 5c). The perforated FPOSS layers lead to the in-plane and out-of-plane correlations observed in the GISAXS pattern.[39,40] This self-assembled morphology is termed three-component perforated lamellae (PL_3), and the corresponding lattice parameters are determined as a = 20.5 nm and b = 32.0 nm. When f_{PS} increases to 0.66 (**F4**), the plan-view TEM BF image (Figure 5d) shows dark in-plane packed cylinders (the PEO domain) superpositioned on a gray net-like pattern (the FPOSS domain). The corresponding cross-sectional image (inset of Figure 5d) reveals that the dark cylinders (the PEO domain) are packed similar to a hexagonal packing with broken

DOI: 10.1021/acsnano.5b06038
ACS Nano 2016, 10, 919−929

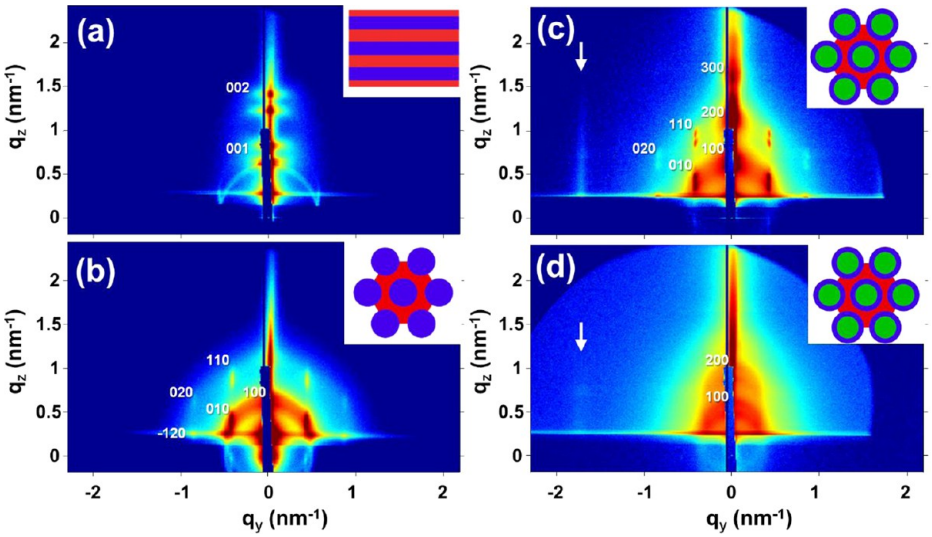

Figure 6. Set of GISAXS patterns at the incident angle of 0.20° of star-like AC_{60}-based (a) A6 and (b) A7 and FPOSS-based (c) F6 and (d) F7 giant surfactants. The insets represent the cross-sectional illustrations for each morphology, with AC_{60} and PEO in blue, PS in red, and FPOSS in green.

gray lines (the FPOSS domain). Different layers of the PEO cylinders are separated by not only the PS matrix but also the perforated FPOSS layers, resulting in a nonhexagonal packing scheme. This complex morphology is termed three-component cylinder-*within*-perforated lamellae (CPL_3), and the overall cross-sectional two-dimensional lattice parallel is determined as a centered rectangular lattice with a = 23.0 nm and b = 35.0 nm. As f_{PS} increases to 0.79 (**F5**), the GISAXS pattern (Figure 3j) shows a similar diffraction pattern to that of **F4** (Figure 3i) but with much lower order, which could be attributed to the higher molecular weight PS blocks that impeded molecular mobility during thermal annealing. Nevertheless, the self-assembled morphology of **F5** may still be deduced as CPL_3 with a = 21.8 nm and b = 34.2 nm, and the low-ordered morphology can be confirmed from both a plan-view and a cross-sectional view of TEM BF images (Figure 5e). Due to the complex structure of CPL_3 for **F4** and **F5**, the length of the PS block does not directly correlate with the size of the 2D lattice. The increment of the PS block could result in a higher degree of perforation in the FPOSS layer and/or a smaller domain size of the PEO cylinders in the 2D lattice.

Notably, diffractions at the high angle region (q_y = 1.7 nm^{-1}) are observed in the GISAXS patterns of **F1** and **F2** (white arrows in Figure 3f and g), which are attributed to the lateral packing of FPOSS with a dimension of 3.6 nm. Higher order diffractions of this lateral packing (white arrows, q_y = 3.4 and 5.1 nm^{-1}) and the scattering attributed to the mesomorphic packing of fluorinated chains (black arrows, q_z = 12.8 nm^{-1}, d-spacing = 0.49 nm) can be observed in the corresponding GIWAXS patterns (Figure S2f and g). These diffractions confirm the mesomorphic nature of the FPOSS with the hepadecafluorodecyl chains oriented parallel to the substrate plane. No diffraction at high-angle regions, however, is observed in the cases of **F3**, **F4**, and **F5**, due probably to the perforated packing and the low volume fraction of FPOSS heads.

Phase Structures in Thin Films of Star-like Giant Surfactants and the Effects of the Architectures. We conducted parallel studies on the star-like giant surfactants to illustrate the importance of molecular topology on the self-assembly. The chemical structure and molecular architecture of star-like giant surfactants are depicted in Figure 2c and d. Four pairs of giant surfactants (**A2**/**A6**, **A4**/**A7**, **F2**/**F6**, and **F4**/**F7**) with identical compositions but different molecular architectures, which are known as topological isomers, are specifically compared. **A6** and **A7** form LAM and HEX morphologies, respectively, based on the GISAXS patterns (Figures 6a and b). The dimension of the LAM morphology of **A6** is 10.8 nm, while the HEX supramolecular lattice of **A7** is 14.6 nm, respectively. The featureless plan-view TEM BF image of **A6** confirms the LAM morphology (Figure 7a). Considering the major component of **A7** is the hydrophobic PS block (f_{PS} = 0.71), the PEO/AC_{60} blocks form hexagonally packed cylinders

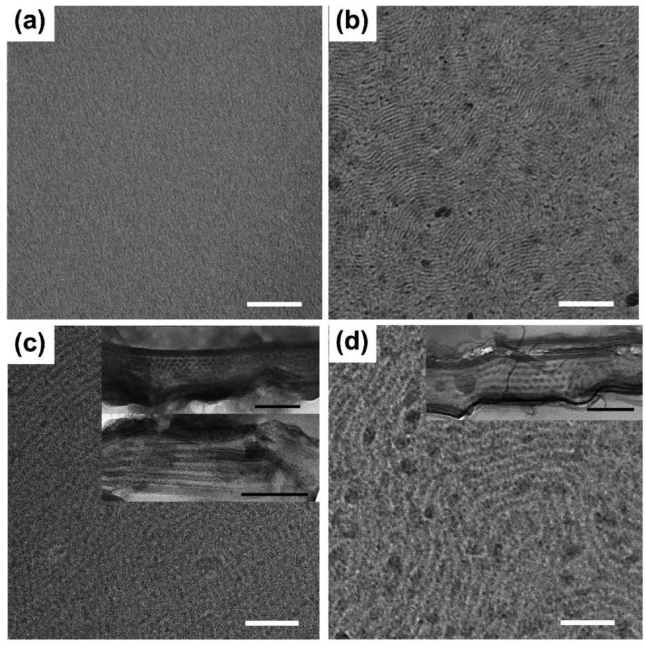

Figure 7. Set of TEM BF images of star-like giant surfactants. Plan-view images of A6 (a), A7 (b), F6 (c), and F7 (d). Insets are corresponding cross-sectional TME images. Scale bar: 100 nm.

DOI: 10.1021/acsnano.5b06038
ACS Nano 2016, 10, 919–929

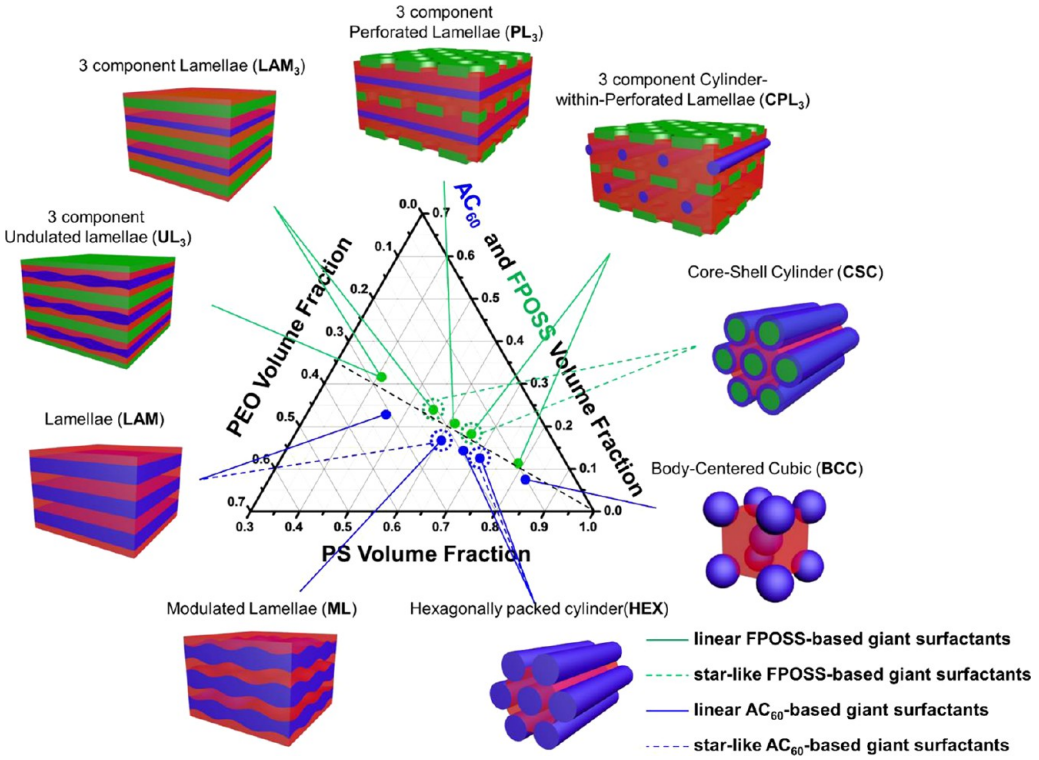

Figure 8. Ternary phase diagram of the overall self-assembly of the giant surfactants. The linear and star-like giant surfactants are depicted by solid and dashed lines, respectively, with blue representing AC_{60}-based giant surfactants and green representing FPOSS-based ones.

that are embedded in the hydrophobic PS matrix. This morphology is further confirmed by the plan-view TEM BF image (Figure 7b), with dark streaks corresponding to the cylindrical PEO/AC_{60} domain. Similar to their linear analogues, the hydrophilic AC_{60} MNPs are dispersed in the PEO/AC_{60} domain without apparent order, as evidenced by the absence of diffraction in the wide-angle region (Figure S3a and b).

The GISAXS pattern of **F6** (Figure 6c) exhibits a typical diffraction pattern of HEX accompanied by an additional diffraction at q_y = 1.7 nm^{-1} (d-spacing = 3.6 nm). The latter has been recognized as the lateral packing of the mesomorphic FPOSS structure along their long axes. The higher order diffractions attributed to the lateral packing of FPOSS and the scattering of mesomorphic packing of fluorinated chains can be observed in the GIWAXS pattern (Figure S3c). On the other hand, the GISAXS pattern of **F7** (Figure 6d) shows two Scherrer–Debye rings with second-ordered diffractions along the q_z direction, indicating a relatively random-oriented morphology. The FPOSS MNPs in this case possess a mesomorphic structure with a short correlation length, according to the diffused diffraction at q_y = 1.7 nm^{-1} (d-spacing = 3.6 nm). The structure of **F7** cannot be determined solely by the GISAXS technique. The structural information provided by TEM in real space will be essential to elucidate the morphology.

The plan-view TEM BF image of **F6** (Figure 7c) clearly shows in-plane aligned cylinders, while the corresponding cross-sectional image confirms the HEX packing scheme in the view perpendicular (upper inset of Figure 7c) and parallel (lower inset of Figure 7c) to the long axes of cylinders. A core–shell cylinder (CSC)[41−43] with a cylindrical core of the FPOSSs (gray) covered by the PEO shell (dark) embedded in the PS matrix (light gray) is speculatively proposed. A similar feature is found in the TEM BF image of **F7** yet, with shorter correlation length (Figure 7d), indicating it also forms CSC structure. The GISAXS patterns can now be indexed correspondingly, and the hexagonal supramolecular lattice is determined as a = 14.8 and 18.3 nm for **F6** and **F7**, respectively. The details of computational fitting for the GISAXS patterns and the corresponding lattice dimensions can be found in Figure S4.

The self-assembled structures of these two sets (linear and star-like) of giant surfactants are summarized in a ternary phase diagram based on the calculated volume fraction of each component (Figure 8). Considering both the MNP component and PEO block have fixed molecular weights and similar volume fractions (Table 1), the experimental data points in the ternary phase diagram are thus reduced near the composition of $f_{PEO} = f_{MNP}$ (the black dashed line in Figure 8). In this case, the role of f_{PS} is accentuated in the phase transition. The AC_{60}-based topological isomer pairs, **A2**/**A6** and **A4**/**A7**, form ML/LAM and HEX/HEX, while the FPOSS-based topological isomer pairs, **F2**/**F6** and **F4**/**F7**, form LAM_3/CSC and CPL_3/CSC.

Stretched PS Block Conformations and Relations to the Phase Stability. Since the AC_{60} and FOSS heads possess fixed interfacial areas, we assume a fixed enthalpy term, $\Sigma\gamma$, where Σ is the interfacial area between the MNP-containing domain and the PS domain and γ is the interfacial tension, in all the structures. The length of the PS block is the only tunable parameter in this study. The morphological phase stability and transformations are critically associated with the conformation of the PS blocks. It is therefore desirable to define a physical quantity that could be used to provide a qualitative correlation between the degree of stretching of the PS blocks and the self-assembled morphology. In order to fulfill this goal, we define a stretching parameter (S) for the PS block. Specifically, the

DOI: 10.1021/acsnano.5b06038
ACS Nano 2016, 10, 919–929

stretching parameter is defined as the ratio between the PS domains and the ideal size of the corresponding PS chain.[28]

$$S = L/R_0 \quad (1)$$

where R_0 is an average end-to-end distance of the unperturbed PS chain that can be calculated based on the degree of polymerization[44] and L is a length characterizing the PS domain (excluding the contribution of both the PEO and the MNPs). The average size of the PS domains, L, for the simple structures corresponding to LAM, HEX, and BCC morphologies can be calculated based on the volume fractions of each block,

$$L = Df_{PS} \quad \text{for LAM} \quad (2)$$

$$L = D\frac{f_{PS}^{2/3}}{f_{PS}^{2/3} + f_{PEO}^{2/3} + f_{MNP}^{2/3}} \quad \text{for HEX} \quad (3)$$

$$L = D\frac{f_{PS}^{1/3}}{f_{PS}^{1/3} + f_{PEO}^{1/3} + f_{MNP}^{1/3}} \quad \text{for BCC} \quad (4)$$

where the characteristic length (D) is measured experimentally, corresponding to the $d_{(001)}$ of LAM, $d_{(100)}$ of HEX, $d_{(100)}$ of BCC, $d_{(020)}$ of ML, and $d_{(002)}$ of LAM_3.

Theoretically, the stretching parameter could be estimated by the L values of the different phases according to the scaling law $L = aN_{PS}^{2/3}$,[11] where the prefactor a for LAM, HEX, and BCC was deduced from the cases of **A1**, **A3**/**A4**, and **A5**, respectively (Table S1). As a general rule, the values of the stretching parameter, S, of the linear giant surfactants are close to unity (Table 2). The structural transition of the linear AC_{60}-based giant surfactants can roughly be understood by comparing the stretching parameter (Figure 9). It is evident that experimentally observed morphologies (circled data points) of **A1**, **A3**, **A4**, and **A5** successively adopt LAM → HEX → BCC morphologies to have S values close to unity (the PS-stretching-free phases). For the case of **A2**, however, the estimated S values of both the LAM and HEX morphology deviate from unity. The ML phase, on the other hand, could partially reduce the level of chain stretching and therefore possesses lower free energy. As a result, **A2** was experimentally observed as a frustrated ML morphology.

In contrast to the linear giant surfactants that exhibit $S \approx 1$, the star-like giant surfactants generally show higher stretching parameters of as high as $S \approx 1.3$ (Table 2). In the case of the AC_{60}-based topological isomer pairs, $S = 1.10$ for the ML phase of linear **A2** and $S = 1.35$ for the LAM phase of star-like **A6**. Because of the linear geometry of **A2**, the midblock of PS can adopt either bridged or looped conformation[45] to accommodate the PS domain in a spacing roughly equal to the end-to-end distance of a single PS chain (Figure 10a), while, due to the star geometry of **A6**, the AC_{60} and PEO blocks of an individual giant surfactant have to locate in the same hydrophilic domain (Figure 10b), and the hydrophobic domain is composed of partially overlapped PS blocks among giant surfactants, resulting in a relatively high stretching parameter (S = 1.35 for **A6**). For the other set of topological isomers, **A4** and **A7** both form a HEX morphology, yet with different domain spacings. The $d_{(100)}$ of **A4** is 10.13 nm with a stretching parameter of 0.98, while the $d_{(100)}$ of **A7** is 14.55 nm with a stretching parameter of 1.41. Again, the PS block in the linear **A4** can adopt either bridged or looped conformation to make the PS domain spacing roughly equal to the end-to-end distance of a single PS block (S = 0.98) (Figure 10c), while the PS domain of star-like **A7** consists of partially overlapped PS blocks, resulting in S = 1.41 (Figure 10d).

For the FPOSS-based topological isomers, although it is impractical to estimate the S for morphologies other than LAM_3 due to the structural complexity, the topological effect on morphology is similar. Linear **F2** and **F4** form LAM_3 and CPL_3, respectively, and their star-like counterparts **F6** and **F7**,

Table 2. Structural Characterization of the Giant Surfactants in a Thin Film

sample	thin film morphology	dimension[a] (nm)	D[b] (nm)	L[c] (nm)	$R_{0,PS}$[d]	S[e]
A1	LAM	(001): 7.90	7.90	3.65	3.62	1.01
A2	ML	(100): 11.30, (001): 17.80	8.90	5.47	4.93	1.10
A3	HEX	(100): 9.35	9.35	5.19	5.47	0.95
A4	HEX	(100): 10.13	10.13	5.95	6.04	0.98
A5	BCC	(100): 16.55	16.55	8.48	8.41	1.01
A6	LAM	(001): 10.80	10.80	6.53	4.83	1.35
A7	HEX	(100): 14.55	14.55	8.54	6.04	1.41
F1	UL_3/LAM_3	(001): 24.02, (100): 16.10/ (001): 14.03			3.62	
F2	LAM_3	(001): 17.02	8.50	4.79	4.93	0.97
F3	PL_3	(100): 20.50, (001): 32.03			5.47	
F4	CPL_3	(100): 23.04, (001): 35.01			6.04	
F5	CPL_3	(100): 21.81, (001): 34.20			8.41	
F6	CSC	(100): 12.81			4.83	
F7	CSC	(100): 13.68			6.04	

[a]Dimension of each morphology, determined by the GISAXS patterns. [b]Characteristic length (D). Due to the structural complexity, the characteristic dimensions for FPOSS-based samples with morphologies other than LAM_3 are not able to be estimated. [c]One-dimensional length (L) of the PS block in each morphology is defined as eqs 2, 3, and 4. [d]Average unperturbed (freely jointed) end-to-end distance (R_0) of the PS block is calculated as $R_0 = (N_{PS}/6.92)^{0.5}b$, where N_{PS} is the degree of polymerization and b is the Kuhn length (b = 1.8 nm for PS).[44] [e]PS block stretching parameter (S).

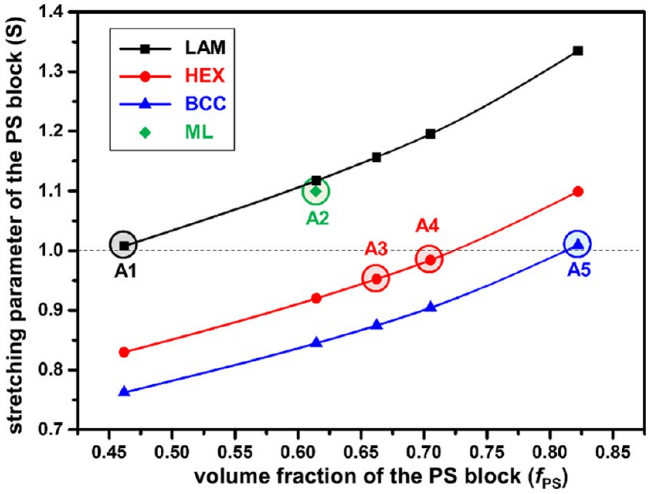

Figure 9. Stretching parameter (S) of the PS block for linear AC_{60}-based giant surfactants at different f_{PS}. Circled data points indicate the experimentally observed morphologies, while the squares, points, and triangles are the calculated values of LAM, HEX, and BCC, respectively.

DOI: 10.1021/acsnano.5b06038
ACS Nano 2016, 10, 919–929

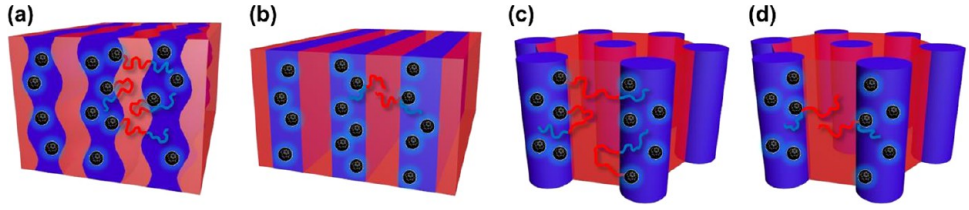

Figure 10. Schematic illustrations of molecular conformations in self-assembled morphologies. (a) ML morphology of linear A2 with bridged and looped midblock PS. (b) LAM morphology of star-like A6. (c) HEX morphology of linear A4 with bridged and looped midblock PS. (d) HEX morphology of star-like A7.

however, both form CSC. In the specific case of CSC, FPOSS cylinders are covered by the collapsed PEO shells with the junction points distributed on the PS/PEO interface (Figure S5).

CONCLUSIONS

New morphologies were observed in thin films of giant surfactants with an AC_{60} or FPOSS head and a block copolymer tail. For linear giant surfactants, the AC_{60}-based samples show two-component morphologies and a transition sequence of LAM → ML → HEX → BCC structures, while three-component morphologies with a morphology transition sequence of UL_3 → LAM_3 → PL_3 → CPL_3 structures are observed in the FPOSS-based samples, with increasing the molecular weight of the PS block. The topological isomers of AC_{60}-based giant surfactants exhibit different dimensions yet in similar or identical morphologies, while those of FPOSS-based giant surfactants show strong topological dependence on the stable morphologies. The stretching parameter of the PS block has been utilized to characterize the bridged/looped chain conformations with $S \approx 1$ for the linear giant surfactants and the partially overlapped chains with $S \approx 1.3$ for the star-like giant surfactants. Due to the A−B−A′ nature of AC_{60}-based giant surfactants, the topological effect only reflects in terms of midblock PS chain conformation, *i.e.*, both bridged and looped PS conformations in the linear giant surfactants and only bridged PS conformation in the star-like giant surfactants. On the other hand, because of the A−B−C nature of FPOSS-based giant surfactants and liquid crystalline FPOSS MNPs, the topological effect is reflected in terms of both the chain conformation and stable morphologies. The versatile self-assembled morphologies suggest that giant surfactants are an excellent platform to produce well-controlled supramolecular structures, and the topology can serve as an additional critical factor to fine-tune the size and the geometry of structures.

METHODS SECTION

Thin Film Preparation. Thin films were prepared by spin coating (Specialty Coating Systems, Inc., spin-coater model P6700) a 1 wt % tetrahydrofuran (THF) solution of giant surfactants at a spin speed of 6000 rpm for 60 s on silicon wafers. The silicon wafer substrates were pretreated with piranha solution (concentrated H_2SO_4/30% H_2O_2 = 3:1 (v/v)) at 80 °C for 30 min, followed by extensive rinsing with deionized water, and then dried under nitrogen flow. The thin films were further annealed at 120 °C under vacuum for 16 h. The thin films were used for grazing incidence X-ray scattering (GIXS) experiments without further treatment, and the same set of thin films were prepared for TEM experiments with a multistep procedure as described below. The film thickness was determined by reflectivity prior to the GIXS measurements (Figure S6 and Table S3). Due to molecular weight and topology differences, the film thickness produced at the same experimental conditions caused some variation. No significant effects of film thickness on the morphologies have been observed.

Grazing Incidence Small-Angle Scattering/Grazing Incidence Wide-Angle Scattering. GISAXS and GIWAXS data were collected at Sector 8-ID-E at the Advanced Photon Source, Argonne National Laboratory.[46] The grazing incidence X-ray scattering patterns were recorded at incident angle of 0.20°, which is between the critical angles of total external reflection for the polymeric film (0.18°) and the silicon wafer (0.245°) in order to maximize the scattering signals from the structures of the entire polymer film. Beamline 8-ID-E operates at an energy of 7.35 keV, and the scattered intensity was collected by a Pilatus 1M-F area detector. GIXS data were analyzed using the GIXSGUI package,[47] and data are corrected for X-ray polarization, detector sensitivity, geometrical solid-angle, *etc.* The beam size is 100 μm (h) × 50 μm (v) and 200 μm (h) × 20 μm (v), and the sample−detector distance is 1400.45 and 204.5 mm for GISAXS and GIWAXS, respectively.

Transmission Electron Microscopy (TEM). TEM experiments were carried out with a JEOL-1230 microscope with an accelerating voltage of 120 kV to record the bright field images. TEM images were taken on a digital CCD camera and processed with the accessory digital imaging software. For enhanced contrast, AC_{60}-based samples were stained by osmium tetroxide (OsO_4) for 16 h and FPOSS-based samples were stained by ruthenium tetroxide (RuO_4) for 10 min. The darkened blotches in some of the TEM images are the artifacts of the staining. To obtain cross-sectional images of the thin films, the thin films on a silicon wafer were first subjected to deposition of a thin layer of amorphous carbon (~20 nm). One drop of a poly(acrylic acid) (PAA) 25% aqueous solution was cast onto the carbon-coated thin film sample. After the solidification of the PAA drop, the thin film was peeled off the silicon wafer by aid of a razor blade. After 20 min of placing the sample onto a distilled water bath with the PAA drop face down, the carbon-coated thin film floated free and was subsequently picked up by a polyimide sheet (125 μm thick). The carbon-coated thin film on the polyimide sheet was then subjected to staining by either OsO_4 or RuO_4. Another layer of carbon was deposited on the stained samples to sandwich the thin films by two layers of amorphous carbon. The samples on the polyimide sheets were further embedded in epoxy (Epofix cold-setting embedding resin, #1232, EMS) and sliced by a microtome (PowerTome PC/CR-X cryosectioning system, RMC) into 80 nm thick slices for TEM observation.

ASSOCIATED CONTENT

Supporting Information

The Supporting Information is available free of charge on the ACS Publications website at DOI: 10.1021/acsnano.5b06038.

Synthetic routes of giant surfactants, mesomorphic structure of FPOSS, GIWAXS patterns, indexed GISAXS patterns, corresponding structural models, and reflectivity data (PDF)

AUTHOR INFORMATION

Corresponding Authors

*E-mail: shi@mcmaster.ca (A.-C. Shi).
*E-mail: elt@rice.edu (E. L. Thomas).

DOI: 10.1021/acsnano.5b06038
ACS Nano 2016, 10, 919−929

*E-mail: scheng@uakron.edu (S. Z. D. Cheng).

Author Contributions

⊥C.-H. Hsu and X.-H. Dong contributed equally.

Notes

The authors declare no competing financial interest.

ACKNOWLEDGMENTS

This work was supported by the National Science Foundation (DMR-1408872). Use of the Advanced Photon Source at Argonne National Laboratory was supported by the U.S. Department of Energy, Office of Science, Office of Basic Energy Sciences, under contract DE-AC02-06CH11357. A.-C.S. is supported by the Natural Science and Engineering Research Council (NSERC) of Canada.

REFERENCES

(1) Sanders, D. P. Advances in Patterning Materials for 193 nm Immersion Lithography. *Chem. Rev.* **2010**, *110*, 321−360.
(2) Pease, F.; Chou, S. Y. Lithography and Other Patterning Techniques for Future Electronics. *Proc. IEEE* **2008**, *96*, 248−270.
(3) Wagner, C.; Harned, N. EUV Lithography: Lithography Gets Extreme. *Nat. Photonics* **2010**, *4*, 24−26.
(4) Hamley, I. W. Nanostructure Fabrication Using Block Copolymers. *Nanotechnology* **2003**, *14*, R39−R54.
(5) Bang, J.; Jeong, U.; Ryu, D. Y.; Russell, T. P.; Hawker, C. J. Block Copolymer Nanolithography: Translation of Molecular Level Control to Nanoscale Patterns. *Adv. Mater.* **2009**, *21*, 4769−4792.
(6) Bates, F. S.; Fredrickson, G. H. Block Copolymer Thermodynamics: Theory and Experiment. *Annu. Rev. Phys. Chem.* **1990**, *41*, 525−557.
(7) Bates, F. S. Polymer-Polymer Phase Behavior. *Science* **1991**, *251*, 898−905.
(8) Bates, F. S.; Hillmyer, M. A.; Lodge, T. P.; Bates, C. M.; Delaney, K. T.; Fredrickson, G. H. Multiblock Polymers: Panacea or Pandora's Box? *Science* **2012**, *336*, 434−440.
(9) Bates, F. S.; Fredrickson, G. H. Block Copolymers—Designer Soft Materials. *Phys. Today* **1999**, *52*, 32−38.
(10) Matsushita, Y.; Mori, K.; Saguchi, R.; Nakao, Y.; Noda, I.; Nagasawa, M. Molecular Weight Dependence of Lamellar Domain Spacing of Diblock Copolymers in Bulk. *Macromolecules* **1990**, *23*, 4313−4316.
(11) Ohta, T.; Kawasaki, K. Equilibrium Morphology of Block Copolymer Melts. *Macromolecules* **1986**, *19*, 2621−2632.
(12) Bates, C. M.; Seshimo, T.; Maher, M. J.; Durand, W. J.; Cushen, J. D.; Dean, L. M.; Blachut, G.; Ellison, C. J.; Willson, C. G. Polarity-Switching Top Coats Enable Orientation of Sub-10-nm Block Copolymer Domains. *Science* **2012**, *338*, 775−779.
(13) Kennemur, J. G.; Yao, L.; Bates, F. S.; Hillmyer, M. A. Sub-5 nm Domains in Ordered Poly(cyclohexylethylene)-Block-Poly(methyl methacrylate) Block Polymers for Lithography. *Macromolecules* **2014**, *47*, 1411−1418.
(14) Cushen, J. D.; Bates, C. M.; Rausch, E. L.; Dean, L. M.; Zhou, S. X.; Willson, C. G.; Ellison, C. J. Thin Film Self-Assembly of Poly(trimethylsilylstyrene-*b*-D,L-lactide) with Sub-10 nm Domains. *Macromolecules* **2012**, *45*, 8722−8728.
(15) Poelma, J. E.; Ono, K.; Miyajima, D.; Aida, T.; Satoh, K.; Hawker, C. J. Cyclic Block Copolymers for Controlling Feature Sizes in Block Copolymer Lithography. *ACS Nano* **2012**, *12*, 10845−10854.
(16) Wurm, F.; Frey, H. Linear-Dendritic Block Copolymers: The State of The Art and Exciting Perspectives. *Prog. Polym. Sci.* **2011**, *36*, 1−52.
(17) Frischknecht, A.; Fredrickson, G. H. Microphase Boundaries and Chain Conformations in Multiply Branched Diblock Copolymers. *Macromolecules* **1999**, *32*, 6831−6836.
(18) Morozov, A. N.; Fraaije, J. G. E. M. Phase Behavior of Block Copolymer Melts with Arbitrary Architecture. *J. Chem. Phys.* **2001**, *114*, 2452−2465.
(19) Glotzer, S. C.; Horsch, M. A.; Iacovella, C. R.; Zhang, Z.; Chan, E. R.; Zhang, X. Self-Assembly of Anisotropic Tethered Nanoparticle Shape Amphiphiles. *Curr. Opin. Colloid Interface Sci.* **2005**, *10*, 287−295.
(20) Zhu, X.; Wang, L.; Lin, J.; Zhang, L. Ordered Nanostructures Self-Assembled from Block Copolymer Tethered Nanoparticles. *ACS Nano* **2010**, *4*, 4979−4988.
(21) Zhang, W.-B.; Yu, X.; Wang, C.-L.; Sun, H.-J.; Hsieh, I.-F.; Li, Y.; Dong, X.-H.; Yue, K.; Van Horn, R.; Cheng, S. Z. D. Molecular Nanoparticles Are Unique Elements for Macromolecular Science: From "Nanoatoms" to Giant Molecules. *Macromolecules* **2014**, *47*, 1221−1239.
(22) Yu, X.; Yue, K.; Hsieh, I.-F.; Li, Y.; Dong, X.-H.; Liu, C.; Xin, Y.; Wang, H.-F.; Shi, A.-C.; Newkome, G. R.; Ho, R.-M.; Chen, E.-Q.; Zhang, W.-B.; Cheng, S. Z. D. Giant Surfactants Provide a Versatile Platform for Sub-10-nm Nanostructure Engineering. *Proc. Natl. Acad. Sci. U. S. A.* **2013**, *110*, 10078−10083.
(23) Mogi, Y.; Mori, K.; Matsushita, Y.; Noda, I. Tricontinuous Morphology of Triblock Copolymers of the ABC Type. *Macromolecules* **1992**, *25*, 5412−5415.
(24) Huang, M.; Hsu, C.-H.; Wang, J.; Mei, S.; Dong, X.; Li, Y.; Li, M.; Liu, H.; Zhang, W.; Aida, T.; Zhang, W.-B.; Yue, K.; Cheng, S. Z. D. Selective Assemblies of Giant Tetrahedra via Precisely Controlled Positional Interactions. *Science* **2015**, *348*, 424−428.
(25) Bailey, T. S.; Pham, H. D.; Bates, F. S. Morphological Behavior Bridging the Symmetric AB and ABC States in the Poly(styrene-*b*-isoprene-*b*-ethylene oxide) Triblock Copolymer System. *Macromolecules* **2001**, *34*, 6994−7008.
(26) Auschra, C.; Stadler, R. New Ordered Morphologies in ABC Triblock Copolymers. *Macromolecules* **1993**, *26*, 2171−2174.
(27) Ni, B.; Dong, X.-H.; Chen, Z.; Lin, Z.; Li, Y.; Huang, M.; Fu, Q.; Cheng, S. Z. D.; Zhang, W.-B. Clicking" Fluorinated Polyhedral Oligomeric Silsesquioxane onto Polymers: A Modular Approach toward Shape Amphiphiles with Fluorous Molecular Clusters. *Polym. Chem.* **2014**, *5*, 3588−3597.
(28) Yu, X.; Zhang, W.-B.; Yue, K.; Li, X.; Liu, H.; Xin, Y.; Wang, C.-L.; Wesdemiotis, C.; Cheng, S. Z. D. Giant Molecular Shape Amphiphiles Based on Polystyrene-Hydrophilic [60]Fullerene Conjugates: Click Synthesis, Solution Self-Assembly, and Phase Behavior. *J. Am. Chem. Soc.* **2012**, *134*, 7780−7787.
(29) Ni, B.; Huang, M.; Chen, Z.; Chen, Y.; Hsu, C.-H.; Li, Y.; Pochan, D.; Zhang, W.-B.; Cheng, S. Z. D.; Dong, X.-H. Pathway toward Large Two-Dimensional Hexagonally Patterned Colloidal Nanosheets in Solution. *J. Am. Chem. Soc.* **2015**, *137*, 1392−1395.
(30) Lin, Z.; Lu, P.; Hsu, C.-H.; Sun, J.; Zhou, Y.; Huang, M.; Yue, K.; Ni, B.; Dong, X.-H.; Li, X.; Zhang, W.-B.; Yu, X.; Cheng, S. Z. D. Hydrogen Bonding Induced Nanophase Separation in Giant Surfactants Consisting of Hydrophilic [60]Fullerene Tethered to Block Copolymers at Different Locations. *Macromolecules* **2015**, *48*, 5496−5503.
(31) Dong, X.-H.; Ni, B.; Huang, M.; Hsu, C.-H.; Chen, Z.; Lin, Z.; Zhang, W.-B.; Shi, A.-C.; Cheng, S. Z. D. Chain-Overcrowding Induced Phase Separation and Hierarchical Structure Formation. *Macromolecules* **2015**, *48*, 7172−7179.
(32) He, J.; Yue, K.; Liu, Y.; Yu, X.; Ni, P.; Cavicchi, K. A.; Quirk, R. P.; Chen, E.-Q.; Cheng, S. Z. D.; Zhang, W.-B. Fluorinated Polyhedral Oligomeric Silsesquioxane-Based Shape Amphiphiles: Molecular Design, Topological Variation, and Facile Synthesis. *Polym. Chem.* **2012**, *3*, 2112−2120.
(33) Lee, B.; Park, I.; Yoon, J.; Park, S.; Kim, J.; Kim, K.-W.; Chang, T.; Ree, M. Structural Analysis of Block Copolymer Thin Films with Grazing Incidence Small-Angle X-Ray Scattering. *Macromolecules* **2005**, *38*, 4311−4323.
(34) Stein, G. E.; Cochran, E. W.; Katsov, K.; Fredrickson, G. H.; Kramer, E. J.; Li, X.; Wang, J. Symmetry Breaking of In-Plane Order in Confined Copolymer Mesophases. *Phys. Rev. Lett.* **2007**, *98*, 158302.
(35) Stein, G. E.; Kramer, E. J.; Li, X.; Wang, J. Layering Transitions in Thin Films of Spherical-Domain Block Copolymers. *Macromolecules* **2007**, *40*, 2453−2460.

DOI: 10.1021/acsnano.5b06038
ACS Nano 2016, 10, 919−929

(36) Ludwigs, S.; Böker, A.; Voronov, A.; Rehse, N.; Magerle, R.; Krausch, G. Self-Assembly of Functional Nanostructures from ABC Triblock Copolymers. *Nat. Mater.* **2003**, *2*, 744−747.
(37) Ludwigs, S.; Schmidt, K.; Krausch, G. One-Dimensional Swelling of A pH-Dependent Nanostructure Based on ABC Triblock Terpolymers. *Macromolecules* **2005**, *38*, 2376−2382.
(38) Park, I.; Park, S.; Park, H.-W.; Chang, T.; Yang, H.; Ryu, C. Y. Unexpected Hexagonally Perforated Layer Morphology of PS-*b*-PMMA Block Copolymer in Supported Thin Film. *Macromolecules* **2006**, *39*, 315−318.
(39) Park, I.; Lee, B.; Ryu, J.; Im, K.; Yoon, J.; Ree, M.; Chang, T. Epitaxial Phase Transition of Polystyrene-*b*-Polyisoprene from Hexagonally Perforated Layer to Gyroid Phase in Thin Film. *Macromolecules* **2005**, *38*, 10532−10536.
(40) Lee, B.; Park, I.; Park, H.; Lo, C.-T.; Chang, T.; Winans, R. E. Electron Density Map Using Multiple Scattering in Grazing-Incidence Small-Angle X-Ray Scattering. *J. Appl. Crystallogr.* **2007**, *40*, 496−504.
(41) Liu, M.; Li, W.; Qiu, F.; Shi, A.-C. Theoretical Study of Phase Behavior of Frustrated ABC Linear Triblock Copolymers. *Macromolecules* **2012**, *45*, 9522−9530.
(42) Tang, P.; Qiu, F.; Zhang, H. D.; Yang, Y. L. Morphology and Phase Diagram of Complex Block Copolymers: ABC Star Triblock Copolymers. *J. Phys. Chem. B* **2004**, *108*, 8434−8438.
(43) Sioula, S.; Hadjichristidis, N.; Thomas, E. L. Novel 2-Dimensionally Periodic Non-Constant Mean Curvature Morphologies of 3-Miktoarm Star Terpolymers of Styrene, Isoprene, and Methyl Methacrylate. *Macromolecules* **1998**, *31*, 5272−5277.
(44) Rubinstein, M.; Colby, R. H. *Polymer Physics*, 1st ed.; Oxford University Press: Oxford, 2003; pp 53−54.
(45) Matsushita, Y.; Nomura, M.; Watanabe, J.; Mogi, Y.; Noda, I.; Imai, M. Alternating Lamellar Structure of Triblock Copolymers of The ABA Type. *Macromolecules* **1995**, *28*, 6007−6013.
(46) Jiang, Z.; Li, X.; Strzalka, J.; Sprung, M.; Sun, T.; Sandy, A. R.; Narayanan, S.; Lee, D. R.; Wang, J. The Dedicated High-Resolution Grazing-Incidence X-Ray Scattering Beamline 8-ID-E at The Advanced Photon Source. *J. Synchrotron Radiat.* **2012**, *19*, 627−636.
(47) Jiang, Z. GIXSGUI: A MATLAB Toolbox for Grazing-Incidence X-Ray Scattering Data Visualization and Reduction, and Indexing of Buried Three-Dimensional Periodic Nanostructured Films. *J. Appl. Crystallogr.* **2015**, *48*, 917−926.

DOI: 10.1021/acsnano.5b06038
ACS Nano 2016, 10, 919−929